Journal of Engineering Science and Technology
Vol. 17, No. 2 (2022) 0936 - 0955

THE EFFECT OF MONSOON ON THE BAY OF BENGAL BASED ON A HYDRODYNAMIC MODEL

YUDI HADITIAR[1], MUTIARA R. PUTRI[2], NAZLI ISMAIL[3], Z.A. MUCHLISIN[4,5], MUHAMMAD IKHWAN[6], MARWAN RAMLI[6], SUGIANTO SUGIANTO[7], REZA WAFDAN[1], MAKWIYAH A. CHALILUDDIN[8], SYAMSUL RIZAL[1,5,*]

[1]Department of Marine Sciences, Faculty of Marine and Fisheries, Universitas Syiah Kuala, Banda Aceh 23111, Indonesia
[2]Department of Oceanography, Bandung Institute of Technology, Bandung 40132, Indonesia
[3]Department of Physics, Universitas Syiah Kuala, Banda Aceh 23111, Indonesia
[4]Department of Aquaculture, Faculty of Marine and Fisheries, Universitas Syiah Kuala, Banda Aceh 23111, Indonesia
[5]Graduate School of Mathematics and Applied Sciences, Universitas Syiah Kuala, Banda Aceh 23111, Indonesia
[6]Department of Mathematics, Universitas Syiah Kuala, Banda Aceh 23111, Indonesia
[7]Department of Soil Science, Faculty of Agriculture, Universitas Syiah Kuala, Banda Aceh 23111, Indonesia
[8]Department of Fisheries Resource Utilization, Faculty of Marine and Fisheries, Universitas Syiah Kuala, Banda Aceh 23111, Indonesia
*Corresponding Author: srizal@unsyiah.ac.id

Abstract

Understanding hydrodynamics in Bay of Bengal (BoB) is crucial because of its connectivity to local extreme weather, ocean fronts, pollutions, and fishing activities. This study aims to describe the hydrodynamics of BoB, including the gyre and the temperature-salinity profile during the monsoon. The research was conducted based on simulating a three-dimensional numerical model, i.e., the HAMburg Shelf Ocean Model (HAMSOM). The model is forced by the tides and meteorological forcing obtained from NCEP/NCAR Reanalysis, which consists of sea level pressure, cloud cover, precipitation, relative humidity, air temperature, zonal and meridional wind. The results showed that the hydrodynamic model (HAMSOM) is quite realistic, according to The Operational Sea Surface Temperature and Sea Ice Analysis (OSTIA) and previous research. OSTIA is a product of a combination of in-situ SST data (Sea Surface Temperature) with reasonably high accuracy. According to the results (HAMSOM), in February (Northeast monsoon), the sea surface currents of BoB are dominated by the poleward East India Coastal Current (EICC) and anticyclone gyres, while the bottom currents are dominated by the reversing EICC originating from near the Andaman Island (more than 300 meters). In this period, atmospheric conditions and sea surface currents support a cold SST and deep mixed layer depth in BoB (reaching 125 meters). In August, the southwest wind is very strong, causing the eastward currents and more gyre in BoB. Also, SST is relatively warm, so the temperature in a vertical direction is more stratified. Compared to the other parts, stratification is very strong in the north of BoB. More stratification at the sea surface is induced by the high precipitation and high SST in August or summer periods. Meanwhile, the stratification of temperature spatially varies due to the gyre and the current circulation. According to the result, it is known that the atmospheric variability of BoB determines the strength of the gyre, coastal currents, and ocean stratification.

Keywords: Current circulation, EICC, HAMSOM, Numerical simulation, SST, Winds.

1. Introduction

Bay of Bengal (BoB) is a deep, semi-enclosed, and high-precipitation waters located in the eastern Indian Ocean [1]. BoB is also known as one of the basins with low salinity in the world because of the surplus of precipitation and freshwater flux, especially during southwest monsoon [2-5].

In general, the surface layer of BoB is controlled by the seasonal reversing winds, namely the northeast monsoon (November-February) and the southwest monsoon (June-September). The peak of Northeast wind occurs in December, while the peak of southwest wind occurs in July-August. In response to this seasonal reversing wind, the surface current circulation also experiences seasonal changes. From February until May, the poleward East Indian Coastal Current (EICC) and anticyclone gyre are observed on the surface of BoB. Meanwhile, during June-August, the surface flow is dominated to the east [6]. According to Paul et al. [7], the monsoon also deals with the coastal Kelvin waves that propagate along the eastern coast of BoB.

In the vertical layer of BoB, previously Kumari et al. [4] have reported that seasonal freshening due to monsoon causes the near-surface layer less saline and stable haline stratification. Seasonal freshening, such as a large river discharge flux, also causes the minimum and maximum barrier layers that occur during April-May and December-February.

The hydrodynamic of BoB is complicated and needs further description. In a previous study, Shetye et al. [8, 9] have carried out limited hydrographic surveys in the western part of BoB. Shetye et al. [9] reported that during March-April, the western boundary current (WBC) leading to the poles in the western part of BoB. Meanwhile, Shetye et al. [8] reported that during southwest monsoon upwelling was indicated along the western part of BoB. Andreas and Detlef [10] also carried out a hydrographic survey by ship drift and satellite altimeter data. They reported that the geostrophic currents of BoB have a substantial seasonal variability leading to local monsoon reversals [10].

The current hydrodynamics plays an important role in the distribution of salinity and freshwater budgets in BoB [11-13]. Mathur et al. [14] and Danpadat et al. [15] said that the crucial currents in BoB are EICC and gyre, which can advent the barrier layers along the Indian coast. According to Shroyer et al. [11], the stratification and mixed layer front of BoB changed in a short-time scale in response to strong atmospheric forces such as northeast monsoon and tropical cyclone. Meanwhile, according to Fousiya et al. [1], besides the freshwater flux and river runoff, the stratification in BoB also depends on the oceanic processes associated with mixing and advection.

BoB is high-risk water because it is vulnerable to flooding, cyclone, and sea-level rise due to the influence of monsoon, high tidal range, river drainage system, and low land topography [16]. Hydrodynamic information such as the Sea Surface Temperature (SST) maximum zone can be useful in studying the formation and tracking of tropical cyclones in BoB [11,17]. According to Khan et al. [18], annual SST in the southern and central parts of BoB have sufficient requirements (SST> 26 ^{o}C) in the genesis of tropical cyclones.

These results showed that the hydrographic data of BoB is still required. Recently, BoB has analysed with a numerical model by Danpadat et al. [15], Jana

et al. [19], Mathur et al. [20], and Dey et al. [21]. They have tested the effects of river run-off on the surface of BoB. They reported that during the monsoon and post-monsoon periods, freshwater from the major rivers of BoB was important to the surface and vertical layers of BoB. However, for better model results, they suggested some improvements, including parameterizations, tides, river discharges, and assimilation data. Therefore, in this study, we use the ocean force from the tides, assimilation data, and meteorological components.

This study explored the hydrodynamics of BoB, including the gyre and the temperature-salinity profile during the monsoon. The research also accommodates the limited information in the deep layer of BoB. Instead of a one-dimensional model, Kantha et al. [22] suggested a three-dimensional model for current advection and SST prediction. Likewise, Narvekar and Kumar [23] proposed a high-resolution model that anticipates limited in situ data and remote sensing for BoB. Therefore, the conducted research was on a simulation of the three-dimensional numerical model (HAMSOM). In this study, the hydrodynamics during northeast monsoon is represented by February and southwest monsoon or summer monsoon by August. The model resulted in the form of circulating currents and temperature-salinity profiles were then compared and studied.

The paper is organized as follows. Section 2 describes the numerical model set up. Section 3 presents the current hydrodynamics, SST, and temperature in the vertical section of BoB.

2. Material and Model Setup

2.1. Data

The depth of the model is obtained from one-minute Shuttle Radar Topography Mission (SRTM30) data (https://topex.ucsd.edu/WWW_html/srtm30_plus.html). The data is then interpolated based on the specified spatial grid (Fig. 1). The open boundary of domain covers parts of the Indian Ocean and the Andaman Sea, which stretches at 78.20 E - 96.70 E and 6.6 N - 24.6 N. Initial temperature and salinity of the model were obtained from Levitus et al. [24] and Levitus and Boyer [25]. Meanwhile, the hydrodynamic forcing is obtained from tidal data as TPXO7.2 [26] and meteorological data from 6-hourly NCEP/NCAR reanalysis data [27]. In this study, we use 11 tidal constituents consisting of M2, S2, N2, K2, K1, O1, P1, Q1, M4, MS4, and MN4 tide.

NCEP data used consist of sea level pressure, cloud cover, precipitation, relative humidity, air temperature, zonal and meridional wind. This meteorological data is used to determine the sea surface fluxes of momentum, heat, and freshwater based on bulk formulas [28]. Numerical simulations are carried out from the beginning of January 2015 with a time-step of 600 seconds.

The results of numerical simulations, such as surface current circulation, are verified by the previous studies. Meanwhile, the sea surface temperature (SST) model is verified by the Group for High-Resolution SST product, the Operational SST and Sea Ice Analysis (GHRSST L4 OSTIA). OSTIA is a multi-scale optimum interpolation product with a spatial resolution of 3 minutes. This product is made from a combination of microwave measurement data and infrared satellite instrument.

This product is based on in-situ SST data obtained from the Global Telecommunications System (GTS) and the EUMETSAT Ocean and Sea Ice

Satellite Applications Facility (OSI SAF). OSTIA was verified by ENVISAT Advanced Along Track Scanning Radiometer (AATSR) SST data and in situ SST measurements from drifting buoys. Based on Donlon et al. [29], the SST's OSTIA product has a zero bias in average and relatively high accuracy. Until now, OSTIA has been continuously monitored and verified. These data can be accessed at (https://podaac.jpl.nasa.gov/dataset/OSTIA-UKMO-L4-GLOB-v2.0).

Figure 1 shows the depth and vertical transects of BoB model. BoB is deep water that covers the waters of India, Bangladesh, and Myanmar. The deepest part of BoB is located at its southern part near the Indian Ocean (can reach 3600 meters). The shallow part of BoB is in the northern part around the coast of Bangladesh (less than 300 meters). The depth contours at the BoB gradually increase from the north to the south. It is different from the Andaman Sea, where the depth is deep and varies strongly.

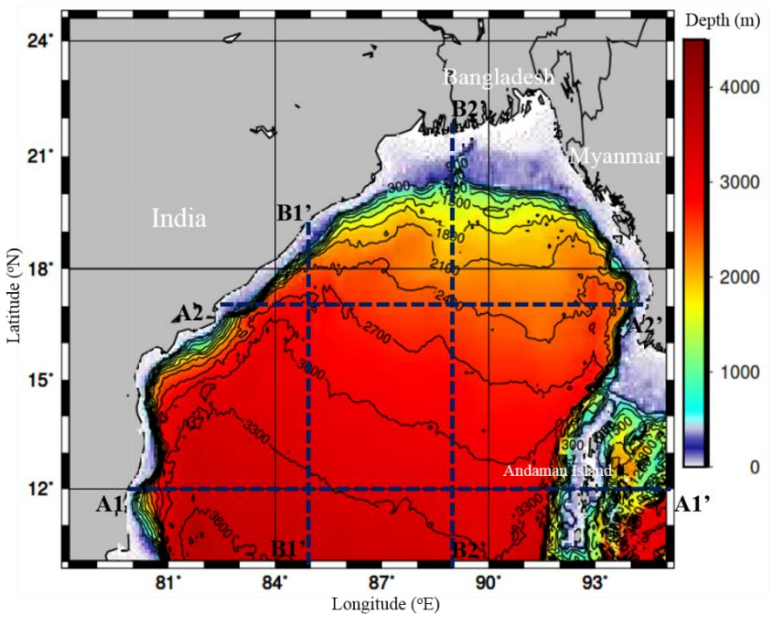

Fig. 1. Domain and bathymetry of Bay of Bengal obtained from SRTM30.

2.2. Model setup

The seawater motion equation used consists of momentum (Eq. (1)), continuity (Eq. (2)), and the transport equation for temperature and salinity (Eqs. (6)-(7)). Simultaneously, the free surface is based on the hydrostatic pressure approach (Eqs. (4)-(5)). To solve Eqs. (1)-(7), we use the HAMburg Shelf Ocean Model (HAMSOM), which is a three-dimensional model with primitive baroclinic equations with a free surface and a hydrostatic approximation [30, 31]. The deduction of the equation can be found in Pohlmann [32]. These equations are defined on the Arakawa C-grid with Z-vertical coordinates and the vertical exchange and diffusivity coefficients determined from the General Ocean Turbulence Model (GOTM).

This model also has a two-time level scheme for time-domain discretization. The prognostic variables such as currents, sea-level elevation, temperature, and

salinity that enter into the implicit algorithm are defined in the two-time level scheme. Semi-implicit algorithms are used in iterating sea surface levels in the horizontal direction and flow shear in the vertical direction. The algorithms overcome the stability of the surface gravity waves and the heat conduction equation. More information about the method can be seen in [30-32].

Momentum equations in x and y directions:

$$\frac{\partial u}{\partial t}+u\frac{\partial u}{\partial x}+v\frac{\partial u}{\partial y}+w\frac{\partial u}{\partial z}-fv=-\frac{1}{\rho}\frac{\partial p}{\partial x}+\frac{\partial}{\partial x}\left(A_H\frac{\partial u}{\partial x}\right)+\frac{\partial}{\partial y}\left(A_H\frac{\partial u}{\partial y}\right)+\frac{\partial}{\partial z}\left(A_v\frac{\partial u}{\partial z}\right)+F_x, \quad (1)$$

$$\frac{\partial v}{\partial t}+u\frac{\partial v}{\partial x}+v\frac{\partial v}{\partial y}+w\frac{\partial v}{\partial z}+fu=-\frac{1}{\rho}\frac{\partial p}{\partial y}+\frac{\partial}{\partial x}\left(A_H\frac{\partial v}{\partial x}\right)+\frac{\partial}{\partial y}\left(A_H\frac{\partial v}{\partial y}\right)+\frac{\partial}{\partial z}\left(A_v\frac{\partial v}{\partial z}\right)+F_y. \quad (2)$$

The left side of Eqs. (1) and (2) consist of the local component, advection terms, and Coriolis force. Meanwhile, the right side consists of pressure gradients due to density, diffusion or turbulence terms, and exterior forcing. Horizontal currents are symbolized by u and v while vertical current by w. The Coriolis parameter is defined by f, density with ρ, and hydrostatic pressure with p. Viscosity coefficients in horizontal and vertical directions are defined by A_H and A_v, respectively, while the horizontal exterior forcings are defined by Fx and Fy.

Continuity equation:

$$\frac{\partial \zeta}{\partial t}+\frac{\partial}{\partial x}\int_{-h}^{\zeta}u\,\partial z+\frac{\partial}{\partial y}\int_{-h}^{\zeta}v\,\partial z=0, \quad (3)$$

where ζ is the sea surface height and h is the seawater depth. The kinematic boundary condition at the sea surface is formulated as follows:

$$\frac{\partial \zeta}{\partial t}=w. \quad (4)$$

The sea surface height is based on a combination of tides and weather calculated from wind and pressure fields [33].

Hydrostatic equation:

$$\frac{\partial p}{\partial z}=\rho g, \quad (5)$$

where g is acceleration of gravity.

The numerical step and solution for Eqs. (1)-(5) can be seen in Rizal [30].

Heat transport equation:

$$\frac{\partial T}{\partial t}+u\frac{\partial T}{\partial x}+v\frac{\partial T}{\partial y}+w\frac{\partial T}{\partial z}=\frac{\partial}{\partial x}\left(K_H^T\frac{\partial T}{\partial x}\right)+\frac{\partial}{\partial y}\left(K_H^T\frac{\partial T}{\partial y}\right)+S_T. \quad (6)$$

Salinity transport equation:

$$\frac{\partial S}{\partial t}+u\frac{\partial S}{\partial x}+v\frac{\partial S}{\partial y}+w\frac{\partial S}{\partial z}=\frac{\partial}{\partial x}\left(K_H^S\frac{\partial S}{\partial x}\right)+\frac{\partial}{\partial y}\left(K_H^S\frac{\partial S}{\partial y}\right)+S_S. \quad (7)$$

Heat and salinity transport (Eqs. (6) and (7)) are caused by the ocean currents advection (Eqs. (1)-(5)). The prognostic of temperatures (T) and salinity (S) are reused in the momentum equation in the baroclinic approximation. On the left side

of the heat and salinity equation, there are local and advection terms. Meanwhile, on the right side consists of diffusion terms and transport sources. Source of heat and salinity are symbolized by S_T and S_S, respectively. In the ocean hydrodynamics model, these sources originated from the sea surface fluxes of momentum, heat, and freshwater. The horizontal Eddy-diffusion coefficient is defined by K_H^T for temperature and K_H^S for salinity. Meanwhile, the vertical eddy-diffusion coefficient are K_v^T and K_v^S.

HAMSOM has been used in modeling physical processes and ocean variability in the North Sea, Andaman Sea, Malacca Strait, and the eastern of Indonesian Waters [31-35]. In this study, the Bay of Bengal (BoB) waters were discretized into $\Delta x = \Delta y = 5$' and 13-layer model. The vertical layer consists of 0-10, 10-20, 20-30, 30-40, 40-50, 50-100, 100-200, 200-300, 300-500, 500-800, 800-1200, 1200- 1800, and > 1800 meters.

3. Results and Discussion

3.1. Wind circulation

The wind is the main force that generates surface circulation in BoB. The wind is also responsible for thermohaline circulation and nutrients in the surface layer of BoB. Figure 2(a) displays wind circulation during February 2015. In February (Northeast Monsoon period), the northeast wind is dominant in BoB. Winds originate from the BoB mainland and head southward to the Indian Ocean and Indian coast. The Northeast wind speed ranges from 4 - 6 m/s, with the strongest part being in the southwest of BoB. In February, an anticyclone with a speed of 4 m/s is observed in the northern part of BoB. Nuncio and Kumar [13] reported that the positive curl in BoB was most influential during the first week of February and dissipated by the second week.

July to August is the peak of the southwest wind on the surface of BoB. Figure 2(b) shows the wind circulation during August 2015. In August, the southwest wind is powerful (can reach 8 m/s) and covers the entire BoB. The speed of the wind is twice higher during August compared to February. Wind circulation reversals in February and August reflect seasonal warming and cooling in northern latitudes.

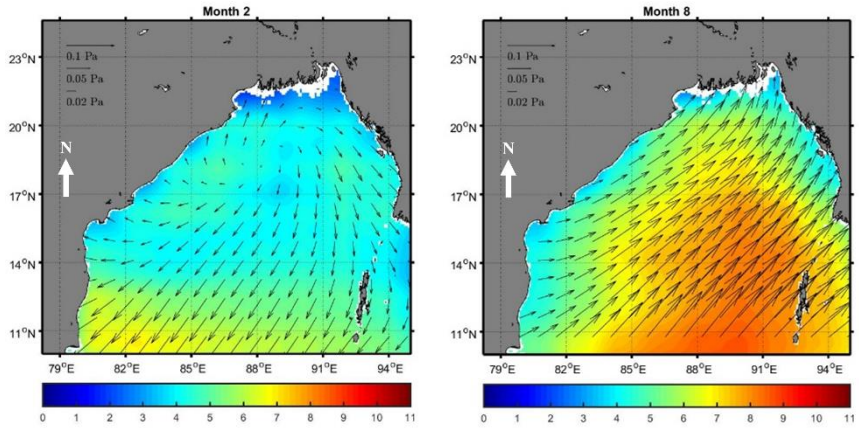

(a) February. **(b) August.**

Fig. 2. (a) The near-sea-surface winds in February and (b) August 2015 obtained from NCEP/NCAR Reanalysis. The shaded colours present the wind speed (in m/s) while the vectors present the wind stress (in Pa).

3.2. Current circulation

Figure 3(a) shows sea surface currents and sea surface height in BoB during February. The current shows a good agreement with the low-resolution currents from Paul et al. [7] and ship-drift observation from Vinayachandran et al. [6]. In February, the Western Boundary Current (WBC), namely the strong East India Coastal Current (EICC), is poleward and anticyclonic gyre flowing in the northern part of BoB (18N-21N). These currents rotate clockwise and flow along the east coast of India, Bangladesh, and western Myanmar because sea level is higher off the coast than in the coastal area. When the currents reach the southern part of the Andaman Islands (around 11N-14N), the currents then turn and join the North Equatorial Current (NEC) heading to the west. The strong northeast wind deflects the currents to the west.

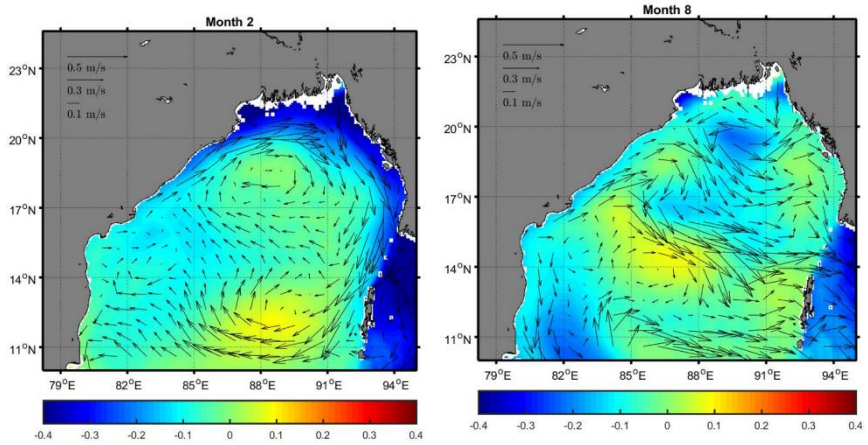

(a) 0-10 m. **(b) 0-10 m.**

Fig. 3. (a) Sea surface height (meter) marked by the colours and sea surface circulation (m/s) shown in vector length in February and (b) August 2015.

Northeast winds also force a low sea surface height near the coast of BoB and part of the Andaman Sea. It causes the currents to tend to be parallel to the coast and flow strongly near the northern coast of BoB. Based on previous results [9, 23], BOB typically has a strong and seasonal WBC peaked during the spring intermonsoon (March-May). Shetye et al. [9] reported that during February-May, anticyclonic gyre enveloping the entire BoB. Based on our results (Fig. 3(a)), anticyclonic gyres are observed in the north (18N-20N and 87E-90E) and south of BoB (11N-13N and 88E-91E).

Figure 3(b) shows the surface currents and sea surface height in August. The current circulation is similar to the observations [6] and the current model from Jana et al. [19]. In August, the surface currents in BoB predominantly flow eastward to the Andaman Sea. Meanwhile, the currents in the Indian coast are divided into two different directions. In the southern part of India, the currents lead the south of BoB. In the northern part of India, currents are diverted eastward to the BoB and the Andaman Sea. In August, cyclone gyres are also observed near the coast of Bangladesh (19-20N and 88-91E).

Anticyclone gyre occurs on the north coast of India (18N-19N and 85E-88E) and in the middle of BoB (13N-15N and 85E-88E). Cyclone gyre causes a low sea

surface around the BoB's mouth, while anticyclone gyre causes a high sea surface in the middle of BoB. In August, the sea surface is relatively low in the Andaman Sea compared to the BoB. By the strong southwest winds, the surface currents from BoB can flow into the Andaman Sea.

Figures 4(a) and 4(b) show the current circulation in February at depths of 100-200 meters and 300-500 meters of BoB, respectively. At a depth of 100-200 meters, a weak anticyclonic gyre and poleward EICC are still observed. It indicates that both current systems work from the surface layer until a depth of 200 meters. The current disappears below 200 meters. At the 100–200-meter layer, the circulation in the Indian coastal (around 17 N) leads to the inshore and is then divided into two directions: the north and south of BoB. This current predominantly flows along the coast of India. At a depth of 300-500 meters, the poleward EICC disappeared and is replaced by the reversing EICC. The currents move from the Andaman Sea, which is the anticyclone gyre area (11N-13N and 88E-91E), to the north and along the coast of BoB. Anticyclone gyre in the south of BoB is relatively strong because it can reach a depth of 500 meters of BoB.

Figures 4(c) and 4(d) show the current circulation in August at depths of 100-200 meters and 300-500 meters of BoB, respectively. The anticyclone gyre is observed until the depth of 500 meters on the north coast of India (18N-19N and 85E-88E). It is also observed in the middle of the BoB (13N-15N and 85E-88E). Between the two gyres is connected by a cyclone gyre (15N-17N and 85E-88E). Meanwhile, at a depth of 300-500 meters, cyclone gyre near the coast of Bangladesh (19-20N and 88-91E) can no longer be observed. Cyclone gyre can only be found to depths of 100-200 meters.

In addition to the gyre feature, counter-current is also observed in the southern part of BoB (10N-11N). This current moves from the east of BoB to the west of BoB. At 83E, this current is deflected to the north and recirculates near the Indian coast (southern part). Thus, in August, the mainstream in the BoB consisted of two anticyclone gyres. Both are in the middle of BoB and a counter-current in the south of BoB. This current circulation rotates inside the BoB and affects the surrounding waters. Meanwhile, only some mass of water from BoB flows into the Andaman Sea. It observed from the surface to a depth of 100 meters.

3.3. Sea surface temperature

Boreal winter from December to February causes SST is low in the northern hemisphere. Figure 5(a) shows sea surface temperature (SST) during February. During February, the lowest SST was observed near the coast of Bangladesh or the northern part of BoB. SST gradually increases from the northern part of BoB to the southern part of BoB and the Andaman Sea (from 25^{o}C to 28^{o}C). This SST (Fig. 5(a)) is quite similar to GHRSST L4 OSTIA (Fig. 5(b)), where SST ranges between 25^{o}C-28 ^{o}C. A low SST also occurs in the northern part of BoB and near the coast of BoB.

Not only the season, but a low SST in BoB is also caused by the surface current circulation that plays a role in delivering cold water masses along BoB coast. The poleward EICC delivers colder SSTs to the Andaman Sea (eastern and south-eastern parts of BoB). On the other hand, the bottom circulation, namely the reversing EICC, delivers water masses from the Andaman Sea to the north and east coast of BoB. These results show how the thermohaline system in BoB works in February.

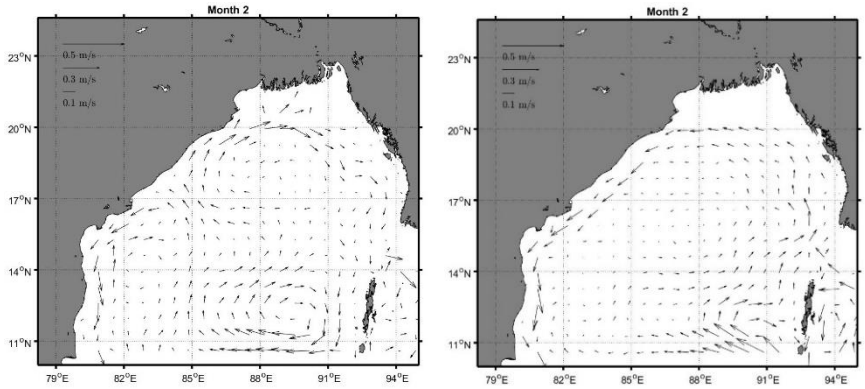

(a) 100-200 m. **(b) 300-500 m.**

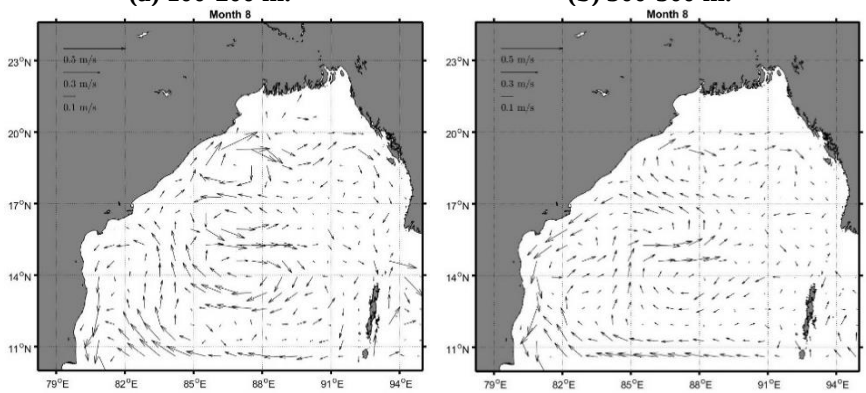

(c) 100-200 m. **(d) 300-500 m.**

Fig. 4. (a-b) Bottom circulation in BoB in February and (c-d) August 2015 (at 100-200 and 300-500 meter).

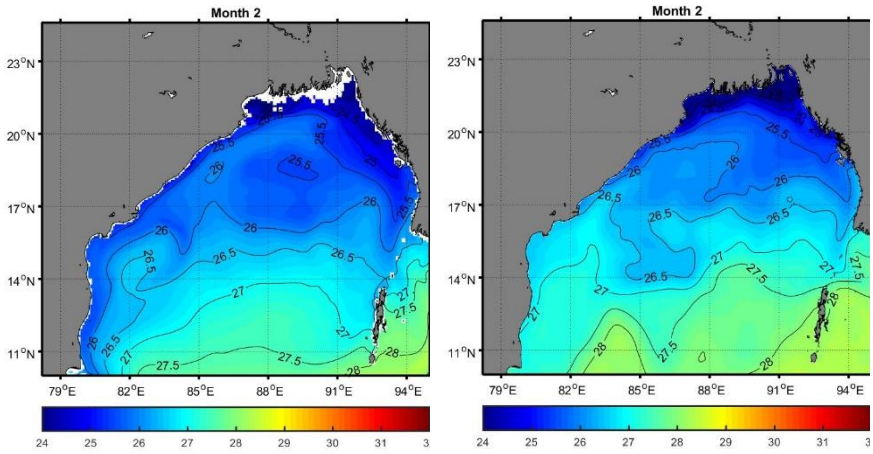

(a) HAMSOM. **(b) OSTIA.**

Fig. 5. (a) Sea surface temperature during February 2015 based on HAMSOM and (b) GHRSST L4 OSTIA.

During summer in August, SST increases in BoB. Figures 6(a) and 6(b) show SST in August from the simulation and GHRSST L4 OSTIA, respectively. The SST simulation result had the range of mean temperature relatively similar to GHRSST L4 OSTIA. During August, SST is quite varied and high (reaching 30ºC) compared to February. According Kantha et al. [22], based on the observational data, during summer months (June-July-August 2015), the SST can reach until 30ºC, at the northern part of BoB. The surface currents carry heat from BoB to the Andaman Sea. The results (Fig. 3(b)) also show that the surface currents heading eastward causes a cold SST on the coast of India and the south-eastern part of Andaman Island.

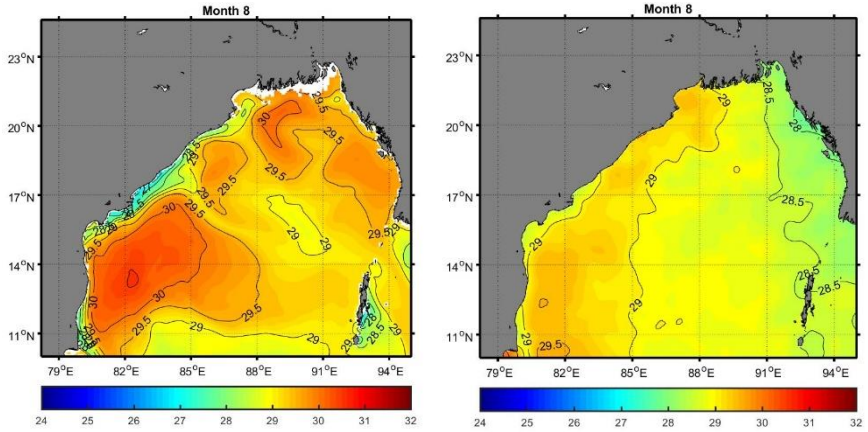

(a) HAMSOM. **(b) OSTIA.**

Fig. 6. (a) Sea surface temperature in August 2015 based on HAMSOM and (b) GHRSST L4 OSTIA.

The presence of gyres in the middle of BoB could also affect SST during August. In addition to gyres and surface currents, SST can also be influenced by the bottom circulation. In the south of BoB, bottom circulation carries colder water from the Andaman Sea to the BoB. This condition is reflected in the cold SST at 10N-11N and 82E-85E which is caused by bottom current circulation. These results are consistent with Shetye et al. [8], where upwelling due to winds formed in the western boundary of BoB during the southwest monsoon (July-August).

3.4. The vertical profiles of BoB

We verified temperature, salinity, and density with prior observations from Kantha et al. [22] and Narvekar and Kumar [23]. These variables are sampled at stations representing the northern part of the BoB and the south of the BoB (see Figs. 7(a-d), Figs. 8(a) and (b), and Figs. 9(a) and (b).

In general, our model shows a good agreement with the observational data derived by Narvekar and Kumar [23]. First, in February and August, in the northern part of the BoB, the isothermal, isohaline, and isopycnal layers are very shallow (Figs. 7(a) and 7(c)), especially in August. Whereas in the southern part of BoB, the isothermal, isohaline, and isopycnal layers are the same, around 50 meters. This is consistent with observations derived by Narvekar and Kumar [23].

Figure 7(a) also showed that the MLD caused by temperature and salinity is different. The MLD difference, caused by temperature, is thicker than that caused by salinity, creating a barrier layer in BoB as found by He et al. [5]. The barrier layer lies below the MLD due to salinity up to the upper limit of the thermocline. Furthermore, He et al. [5] argue that the barrier layer in BoB occurs when winter due to anticyclonic eddies and salinity-stratified oceans. Our review is supportive of the facts presented by He et al. [5], as seen in Figs. 1(a) and 7(a).

Second, in the southern part of the BoB (Figs. 7(b) and 7(d)), regardless of season (February or August), isothermal, isohaline, and isopycnal in the surface layer have the same depth. In August, the thickness of isothermal, isohaline, and isopycnal values is the same, around 50 meters. Thus, in the southern part of the BoB, according to HAMSOM, monsoon replacement is relatively small affecting isothermal, isohaline, and isopycnal thickness.

The cold winter and SST during February made the isotherm in the northern part of the BoB quite deep. But this has less effect on isotherms in the southern part of the BoB. In August, the BoB experienced warm air conditions accompanied by peak precipitation and freshwater fluxes. During this period the thermocline, halocline, and pycnocline can be observed in the upper north of BoB (Fig. 7(c)). The gradients of these layers are stronger than the layers in the southern part of the BoB. A comparison between these two stations reflects that stratification tends to be stronger in the northern part of the BoB than the southern part of the BoB (Fig. 7(d)). Strong stratification in the northern part of the BoB is closely related to the contribution of freshwater from the surrounding rivers. The northern part of the BoB is connected to five major rivers such as Irrawaddy, Ganges, Brahmaputra, Mahanad, and Godavari which can increase freshwater intrusion into the BoB [21]. The magnitude of salinity intrusion causes pycnocline in the northern part of the BoB (at a depth of 50-125 m) to be quite sensitive to changes in salinity.

Figure 8(a) shows temperature in the upper layers of BoB at 18.0167N, 89.5333E from January 1, 2015, to December 31, 2015. In February, the temperature at the top is around 26-27 ^{o}C, whereas in August the temperature can reach more than 29^{o}C. The temperature produced by HAMSOM, is almost the same as observation [22]. Isotherm is deep (can reach 125 m) during winter (December-February) and shallow (less than 15 m) during spring to summer (March-September).

Our model also shows a good result compared to OSTIA and observations from Kantha et al. [22]. In the northern part of the BoB, SST is quite cold during February and warm in August. The isotherm in the northern part of the BoB was quite deep during February compared to August. Meanwhile, in August, the thermocline is in a shallower layer.

Salinity in the upper layers of BoB at 18.0167N, 89.5333E from January 1, 2015, to December 31, 2015, is shown in Fig. 8(b). In layers to a depth of 125 m, it appears that salinity ranges 31.5-35. In February salinity has a value of around 31.5 at the surface, while in August the salinity at the surface reaches 32.5. Isohaline becomes deep during winter (December-February) and shallow during summer (June-September). In general, the pattern formed in this figure is almost the same as the model and observation obtained by Kantha et al. [22].

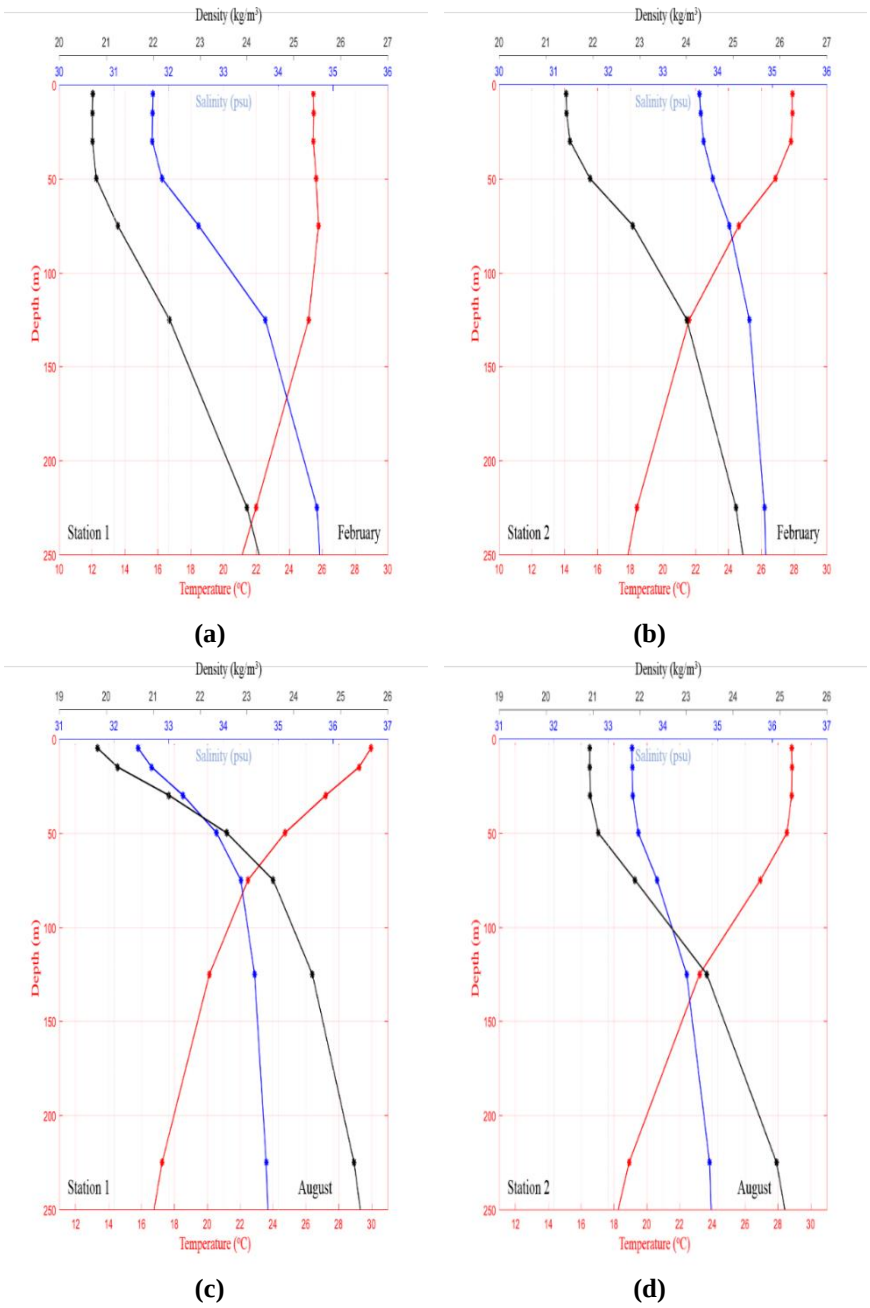

Fig. 7. (a-b) Temperature (red line), salinity (blue line), and density (sigma-t) (black line) in the northern of BoB or Station 1 (19.0167N, 89.0333E) and southern of BoB or Station 2 (9.0167N, 89.0333E), respectively, in February and (c-d) The same as 7(a-b), but for August 2015. Density was calculated from IES-80 [36].

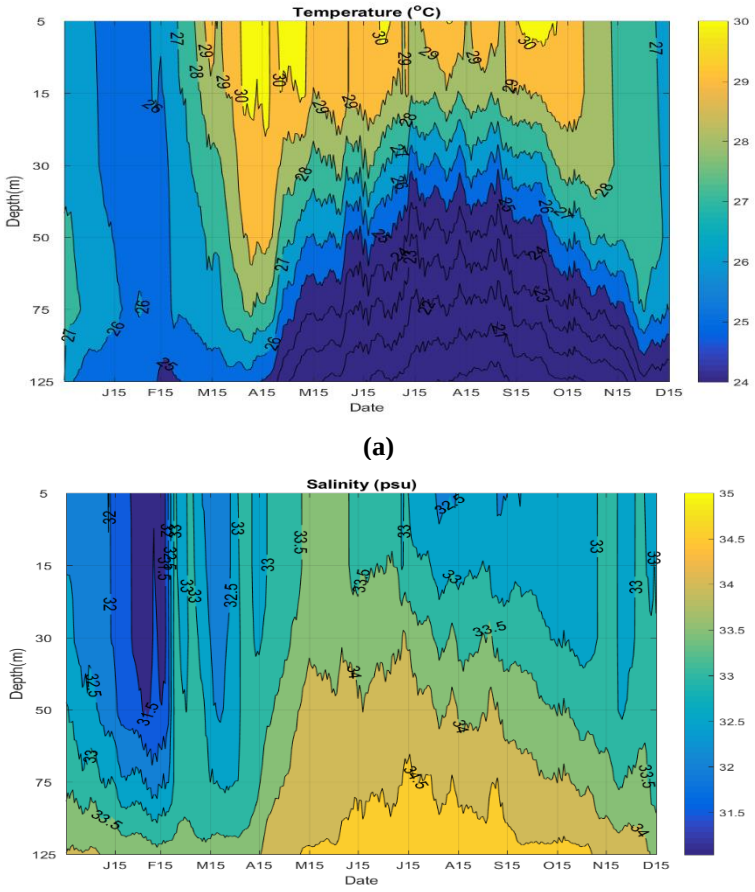

(a)

(b)

Fig. 8. (a) Temperature and (b) salinity in the upper layers of BoB at 18.0167N, 89.5333E from January 1, 2015, to December 31, 2015.

Isohaline in the northern part of the BoB is relatively deep during February and shallow during August. In August, salinity varied greatly, where salinity was very low in the surface layer and high in the lower layer, indicating a strong halocline in the northern part of the BoB (see Fig. 8(b)).

Figure 9(a) shows SST at 18.0167 N, 89.5333 E from January 1, 2015, to December 31, 2015. In general, the SST pattern formed by HAMSOM is almost the same as the pattern of OSTIA. Whereas Fig. 9(b) shows the SSS produced by HAMSOM. This SSS pattern is also similar to the results of the model from Kantha et al. [22]. The mean value of SSS is around 32.5 [22].

Figure 10(a) to (h) shows the vertical section of temperature along the BoB. In general, mixed layer depth is cooler and deeper during February than August. Mixed layer depth based on temperature in February can reach 100 meters while in August only reaches 50 meters. Conversely the thermocline is relatively shallower in August compared to February. In meridional and zonal section, temperatures in August are more varied.

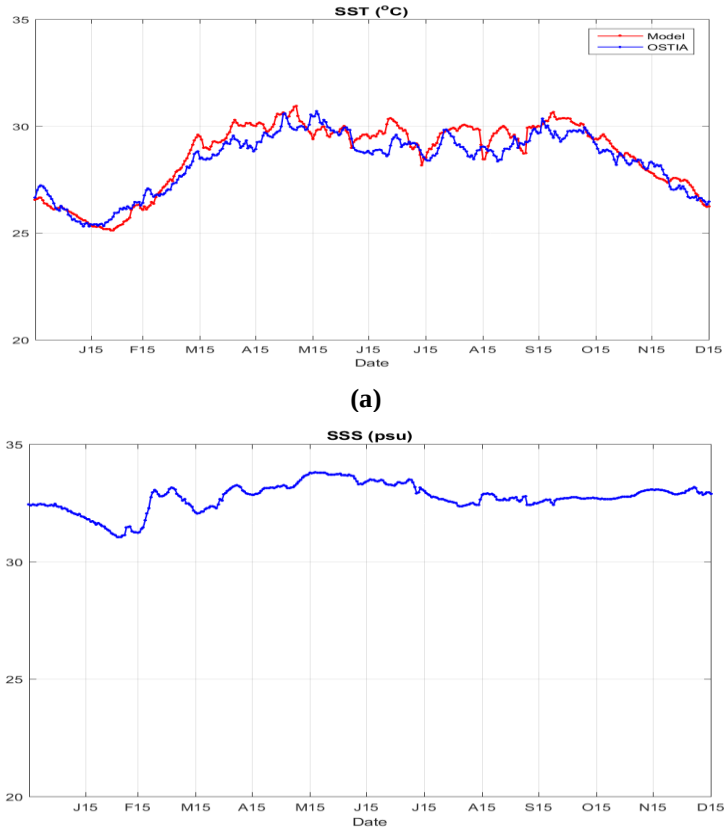

Fig. 9. (a) SST of BoB at 18.0167 N, 89.5333 E from January 1, 2015, to December 31, 2015. The red line presents HAMSOM while the blue line presents OSTIA. (b) SSS at 18.0167N, 89.5333E from January 1, 2015, to December 31, 2015.

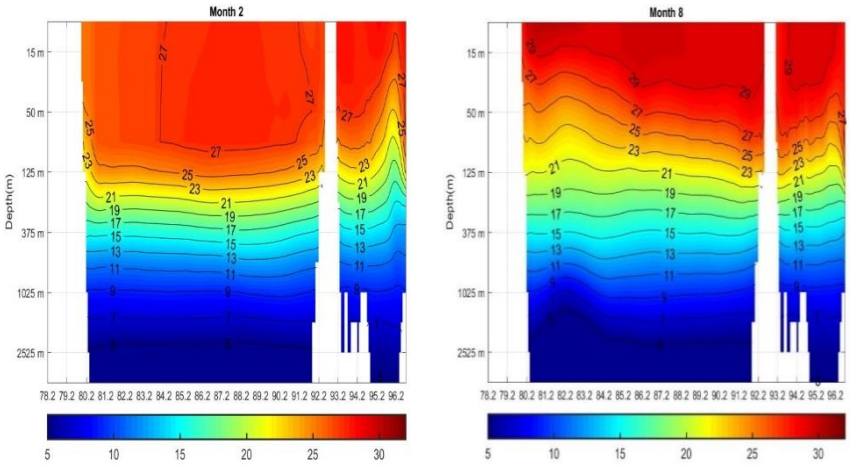

(a) A1-A1' (in February). **(b) A1-A1'(in August).**

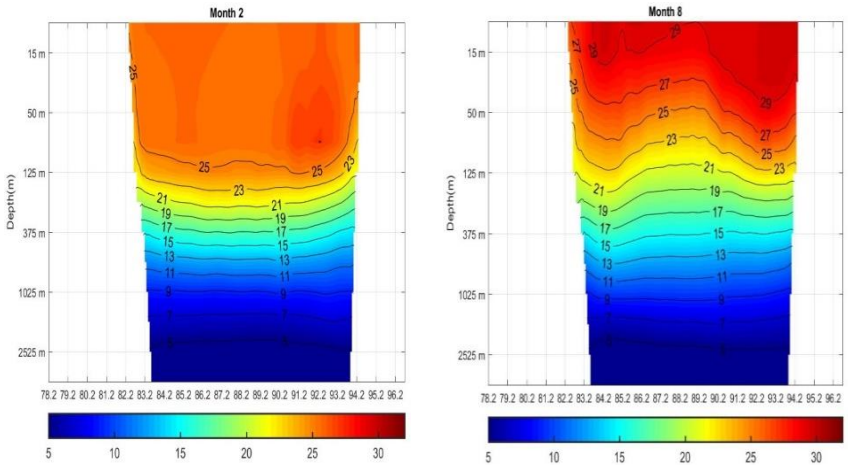

(c) A2-A2' (in February). **(d) A2-A2'(in August).**

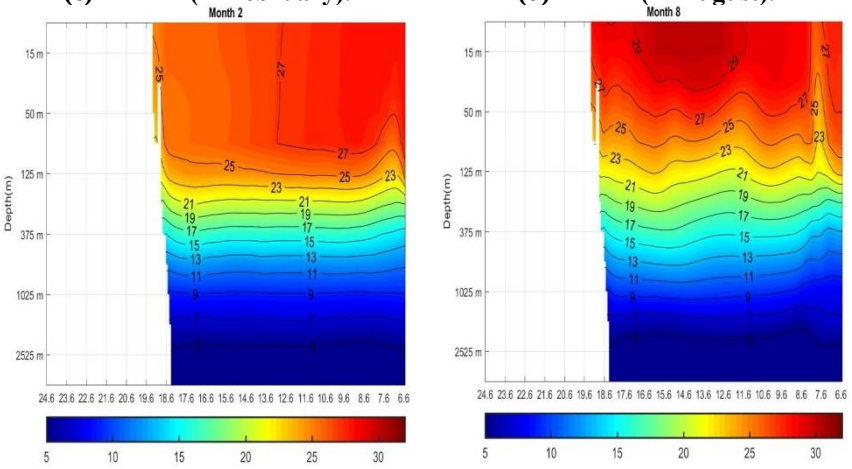

(e) B1-B1' (in February). **(f) B1-B1'(in August).**

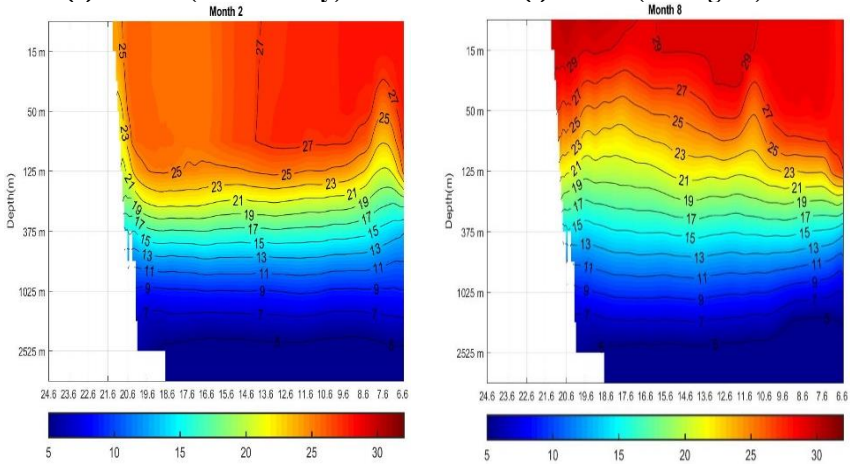

(g) B2-B2' (in February). **(h) B2-B2'(in August).**

Fig. 10. (a-b) Vertical section of temperature along BoB at 12N (A1-A1'), (c-d) 17N (A2-A2'), (e-f) 85E (B1-B1'), and (g-h) 90E (B2-B2') (see Fig.1).

In February, the poleward EICC carrying cold water into BoB. This current affects most temperatures in BoB. It is showed in the homogeneous temperature in the surface layer (0-125 meters). It observed in the meridional transect along 12N in Fig. 10(a) and 17 N in Fig. 10(c). It also observed in the zonal transect along 85E in Fig. 10(e) and along 89.0333E in Fig. 10(g).

Sufficient heat intensity and high precipitation during August caused the BoB to be more stratified. Meanwhile, the presence of gyre and thermohaline circulation causes temperatures in the BoB surface (0-125 meters) to be varied in meridional (along 12N in Fig. 10(b) and along 17N in Fig. 10(d)) and zonal (along 85E in Fig. 10(f) and 89.0333E in Fig. 10(h)). While in February, the influence of currents and winter conditions led to the vertical layer of BoB more homogeneous. During February, the stratification and thermocline are found at a depth of 125 meters.

4. Summary and Conclusion

This paper presents BoB hydrodynamics based on the tidal and monsoon forcing in February and August 2015, which are the northeast monsoon and southwest monsoon periods, respectively. The results of the hydrodynamic model are quite similar to the verification data and previous research. In general, monsoon as atmospheric forcing strongly affects the current circulation, SST, and vertical section of temperature in the BoB. Based on the results, it is known that in February, EICC and two anticyclonic gyres were occurred in the BoB.

The gyres occur in the north (18N-20N and 87E-90E) and south of BoB (11N-13N and 88E-91E). This circulation supports the North Equatorial Current, which leads west to the south of BoB. In the northern part of BoB, the poleward EICC and gyres can reach a depth of 200 meters while in the southern part of BoB, the gyre can reach a depth of 500 meters. These results are entirely in line with the influence of the east wind, which is getting stronger in the southern part of BoB. In February, a thermohaline circulation occurs in BoB. Below the depth of 300 meters, EICC moves in the opposite direction. It is directed from the Andaman Sea to the Indian coast.

In general, in February, the surface of BoB is relatively cold, especially in the northern part. EICC and anticyclonic gyre distribute the cold water (0-200 meters) from the northern part towards the southern part of BoB and its surroundings. As a result, the mixed layers of BoB are deeper in February. In August, the current circulation dominantly flows to the east of BoB and can reach part of the Andaman Sea. During this month, more gyres and strong currents occur in BoB. Gyre and counter-current in BoB can be observed to a depth of 500 meters.

Current circulation supports upwelling potential on the east coast of India. During August, SST is quite varied and high. The sufficient heat intensity and high precipitation causes BoB more stratified in August compared to February. Meanwhile, the strong currents and gyres in August cause temperature stratification spatially varied.

Acknowledgement

This research is funded by Ministry of Education and Culture through the scheme of 'Penelitian Terapan Unggulan Perguruan Tinggi (PTUPT)' with the contract number 11/UN11.2.1/PT.01.03/DPRM/2021.

Nomenclatures

A_H, A_v	Viscosity coefficients in horizontal and vertical directions, m^2/s
f	Coriolis parameter, s^{-1}
F_x, F_y	Exterior forcing in *x*-momentum and y-momentum
g	Acceleration of gravity, m/s^2
h	Seawater depth measured from undisturbed water surface, m
K_H^T, K_H^S	Eddy-diffusion coefficients in horizontal direction, m^2/s
K_v^T, K_v^S	Eddy-diffusion coefficients in vertical direction, m^2/s
p	Hydrostatic pressure, $kg/m/s^2$
S, S_S	Salinity and source of salinity, non-dimensional
T, S_T	Temperature and source of temperature, ^oC
u, v	Horizontal velocity, m/s
w	Vertical velocity, m/s

Greek Symbols

Δt	Numerical time-step, s
Δx, Δy	Horizontal resolution, m
Δz	Vertical resolution, m
ζ	Sea surface height, m
ρ	Seawater density, kg/m^3

Abbreviations

AATSR	Advanced Along Track Scanning Radiometer
BoB	Bay of Bengal
EICC	East India Coastal Current
GODAS	Global Data Assimilation System
GOTM	General Ocean Turbulence Model
GTS	Global Telecommunications System
HAMSOM	HAMburg Shelf Ocean Model
NCEP/NCAR	National Centers for Environmental Prediction/ National Center for Atmospheric Research
OSI SAF	Ocean and Sea Ice Satellite Applications Facility
OSTIA	The Operational SST and Sea Ice Analysis
SRTM	Shuttle Radar Topography Mission
SST	Sea Surface Temperature
SSS	Sea Surface Salinity
WBC	Western Boundary Current

References

1. Fousiya, T.S.; Parekh, A.; and Gnanaseelan, C. (2016). Interannual variability of upper ocean stratification in Bay of Bengal: Observational and modeling aspects. *Theoretical and Applied Climatology*, 126, 285-301.
2. Varkey, M.J.; Murty, V.S.N.; and Suryanarayana, A. (1996). Physical oceanography of the Bay of Bengal and Andaman Sea. *Oceanography and Marine Biology: An Annual Review*, 34, 1-70.

3. Mao, J.; and Wu, G. (2007). Interannual variability in the onset of the summer monsoon over the Eastern Bay of Bengal. *Theoretical and Applied Climatology*, 89, 155-170.
4. Kumari, A.; Kumar, S.P.; and Chakraborty, A. (2018). Seasonal and interannual variability in the barrier layer of the Bay of Bengal. *Journal of Geophysical Research: Oceans*, 123, 1001-1015.
5. He, Q.; Zhan, H.; and Cai, S. (2020). Anticyclonic eddies enhance the winter barrier layer and surface cooling in the Bay of Bengal. *Journal of Geophysical Research: Oceans*, 125, e2020JC016524.
6. Vinayachandran, P.N; Shetye, S.R.; Sengupta, D.; and Gadgil, S. (1996). Forcing mechanisms of the Bay of Bengal circulation. *Current Science*, 71, 753-763.
7. Paul, S.; Chakraborty, A.; Pandey, P.C.; Basu, S.; Stsangi, S.K.; and Ravichandran, M. (2009). Numerical simulation of Bay of Bengal circulation features from ocean general circulation model. *Marine Geodesy*, 32, 1-18.
8. Shetye, S.R.; Shenoi, S.S.C.; Gouveia, A.D.; Michael, G.S.; Sundar, D.; and Nampoothiri, G. (1991). Wind-driven coastal upwelling along the western boundary of the Bay of Bengal during the southwest monsoon. *Continental Shelf Research*, 11, 1397-1408.
9. Shetye, S.R.; Gouveia, A.D.; Shenoi, S.S.C.; Sundar, D.; Michael, G.S.; and Nampoothiri, G. (1993). The western boundary current of the seasonal subtropical gyre in the Bay of Bengal. *Journal of Geophysical Research*, 98, 945-954.
10. Andreas, E.; and Detlef, Q. (2000). Seasonal variability of the Bay of Bengal circulation inferred from TOPEX/Poseidon altimetry. *Journal of Geophysical Research: Oceans*, 105, 3243-3252.
11. Shroyer, E.L.; Gordon, A.L.; Jaeger, G.S.; Freilich, M.; Waterhouse, A.F.; Farrar, J.T.; Sarma, V.V.S.S.; Venkatesan, R.; Weller, R.A.; Moum, J.N.; and Mahadevan, A. (2020). Upper layer thermohaline structure of the Bay of Bengal during the 2013 northeast monsoon. *Deep-Sea Research Part II: Topical Studies in Oceanography*, 172, 104630.
12. Vinayachandran, P.N.; and Kurian, J. (2007). Hydrographic observations and model simulation of the Bay of Bengal freshwater plume. *Deep-Sea Research Part I: Oceanographic Research Papers*, 54, 471-486.
13. Nuncio, M.; and Kumar, S.P. (2012). Life cycle of eddies along the western boundary of the Bay of Bengal and their implications. *Journal of Marine Systems*, 94, 9-17.
14. Mathur, M.; David, M.J.; Sharma, R.; and Agarwal, N. (2019). Thermal fronts and attracting Lagrangian Coherent structures in the north Bay of Bengal during December 2015 - March 2016. *Deep-Sea Research Part II: Topical Studies in Oceanography*, 168, 104636.
15. Dandapat, S.; Gnanaseelan, C.; and Parekh, A. (2020). Impact of excess and deficit river runoff on Bay of Bengal upper ocean characteristics using an ocean general circulation model. *Deep-Sea Research Part II: Topical Studies in Oceanography*, 172, 104714.

16. Sreejith, L.R.; and Bhaskaran, P.K. (2017). Tidal asymmetry and characteristics of tides at the head of the Bay of Bengal. *Quarterly Journal of the Royal Meteorological Society*, 143, 2735-2740.
17. Mohanty, S.; Nadimpalli, R.; Osuri, K.K.; Pattanayak, S.; Mohanty, U.C.; and Sil, S. (2019). Role of sea surface temperature in modulating life cycle of tropical cyclones over Bay of Bengal. *Tropical Cyclone Research and Review*, 8, 68-83.
18. Khan, T.M.A.; Quadir, D.A.; Murty, T.S.; and Sarker, M.A. (2004). Seasonal and interannual sea surface temperature variability in the coastal cities of arabian sea and Bay of Bengal. *Natural Hazards*, 31, 549-560.
19. Jana, S.; Gangopadhyay, A.; Lermusiaux, P.F.J.; Chakraborty, A.; Sil, S.; and Haley, P.J. (2018). Sensitivity of the Bay of Bengal upper ocean to different winds and river input conditions. *Journal of Marine Systems*, 187, 206-222.
20. Mathur, M.; David, M.J.; Sharma, R.; and Agarwal, N. (2019). Thermal fronts and attracting Lagrangian Coherent structures in the north Bay of Bengal during December 2015 - March 2016. *Deep-Sea Research Part II: Topical Studies in Oceanography*, 168, 104636.
21. Dey, S.P.; Dash, M.K.; Sasmal, K.; Jana, S.; and Raju, N.J. (2020). Impact of river runoff on seasonal sea level, Kelvin waves, and East India coastal current in the Bay of Bengal : A numerical study using ROMS. *Regional Studies in Marine Science*, 35, 101214.
22. Kantha, L.; Weller, R.A.; Farrar, J.T.; Rahaman, H.; and Jampana, V. (2019). A note on modeling mixing in the upper layers of the Bay of Bengal : Importance of water type, water column structure and precipitation. *Deep-Sea Research Part II: Topical Studies in Oceanography*, 168, 104643.
23. Narvekar, J.; and Kumar, S.P. (2014). Mixed layer variability and chlorophyll a biomass in the Bay of Bengal. *Biogeosciences Discussions*, 11, 3819-3843.
24. Levitus, S.; Burgett, R.; and Boyer, T.P. (1994). World Ocean Atlas 1994, Volume 3: Salinity. Washington D.C.: NOAA Atlas NESDIS 3. U.S. Department of Commerce.
25. Levitus, S.; and Boyer, T.P. (1994). World ocean atlas 1994. Volume 4: Temperature. Washington D.C.: NOAA Atlas NESDIS 4. U.S. Department of Commerce.
26. Egbert, G.D.; Erofeeva, S.Y.; and Ray, R.D. (2010). Assimilation of altimetry data for nonlinear shallow-water tides: Quarter-diurnal tides of the Northwest European shelf. *Continental Shelf Research*, 30, 668-679.
27. Kalnay, E.; Leetmaa, A.; Ropelewski, C.; Deaven, D.; Joseph, D.; White, G.; Janowiak, J.; Wang, J.; Woollen, J.; Mo, K.C.; Gandin, L.; Chelliah, M.; Iredell, M.; Kanamitsu, M.; Jenne, R.; Kistler, R.; Reynolds, R.; Saha, S.; Collins, W.; Ebisuzaki, W.; Higgins, W.; Zhu, Y.; Deaven, D.; Gandin, L.; Iredell, M.; Saha, S.; White, G.; Woollen, J.; Zhu, Y.; Leetmaa, A.; Reynolds, R.; Chelliah, M.; Ebisuzaki, W.; Higgins, W.; Janowiak, J.; Mo, K.C.; Ropelewski, C.; Wang, J.; Jenne, R.; and Joseph, D. (1996). The NCEP/NCAR 40-year reanalysis project. *Bulletin of the American Meteorological Society*, 77, 437-471.

28. Meyer, E.M.; Pohlmann, T.; and Weisse, R. (2009). *Hindcast simulation of the North Sea by HAMSOM for the period of* 1948 *till* 2007 - *Temperature and heat content*. Germany: GKSS Research Centre Geesthacht GmbH.
29. Donlon, C.J.; Martin, M.; Stark, J.; Roberts-jones, J.; Fiedler, E.; and Wimmer, W. (2012). The operational sea surface temperature and sea ice analysis (OSTIA) system. *Remote Sensing of Environment*, 116, 140-158.
30. Rizal, S. (2000). The role of non-linear terms in the shallow water equation with the application in three-dimensional tidal model of the Malacca Strait and Taylor's problem in low geographical latitude. *Continental Shelf Research*, 20, 1965-1991.
31. Rizal, S.; Damm, P.; Wahid, M.A.; Sündermann, J.; Ilhamsyah, Y.; Iskandar, T.; and Muhammad. (2012). General circulation in the Malacca Strait and Andaman Sea: A numerical model study. *American Journal of Environmental Sciences*, 8, 479-488.
32. Pohlmann, T. (1996). Calculating the development of the thermal vertical stratification in the North Sea with a three-dimensional baroclinic circulation model. *Continental Shelf Research*, 16, 163-194.
33. Mayer, B.; Damm, P.E.; Pohlmann, T.; and Rizal, S. (2010). What is driving the ITF? An illumination of the Indonesian throughflow with a numerical nested model system. *Dynamics of Atmospheres and Oceans*, 50, 301-312.
34. Putri, M.R.; and Pohlmann, T. (2012). *Hydrodynamic and Transport Model of the Siak Estuary, in: Subramanian, V.* (*Ed.*), *Coastal Environments: Focus on Asian Regions*. Dordrecht: Springer Netherlands.
35. Putri, M.R.; and Pohlmann, T. (2014). Lagrangian model simulation of passive tracer dispersion in the Siak Estuary and Malacca Strait. *Asian Journal of Water, Environment and Pollution*, 11, 67-74.
36. Sideney, B.C. (1981). Tenth report of the joint panel on océanographie tables and standards (JPOTS). *UNESCO Technical Papers in Marine Science*, 36, 1-25.